Applied Physics A (2018) 124:233
https://doi.org/10.1007/s00339-018-1644-z

Applied Physics A
Materials Science & Processing

The effect of different thickness alumina capping layers on the final morphology of dewet thin Ni films

Benjamin C. White[1] · Amir Behbahanian[1] · T. McKay Stoker[1] · Jason D. Fowlkes[2] · Chris Hartnett[3] · Phillip D. Rack[2,3] · Nicholas A. Roberts[1]

Received: 4 December 2017 / Accepted: 1 February 2018
© Springer-Verlag GmbH Germany, part of Springer Nature 2018

Abstract
Nanoparticles on a substrate have numerous applications in nanotechnology, from enhancements to solar cell efficiency to improvements in carbon nanotube growth. Producing nanoparticles in a cost effective fashion with control over size and spacing is desired, but difficult to do. This work presents a scalable method for altering the radius and pitch distributions of nickel nanoparticles. The introduction of alumina capping layers to thin nickel films during a pulsed laser-induced dewetting process has yielded reductions in the mean and standard deviation of radii and pitch for dewet nanoparticles with no noticeable difference in final morphology with increased capping layer thickness. The differences in carbon nanotube mats grown, on the uncapped sample and one of the capped samples, is also presented here, with a more dense mat being present for the capped case.

1 Introduction

Nanostructured materials present a promising route to both enable a broad range of new technology applications as well as make improvements upon existing technologies. Some examples include flexible sensors or electronic skin based on nanoparticles [1], polymeric nanostructures for atmospheric water condensation [2] or improvements to solar cell efficiency via plasmonic nanoparticles [3–5]. Another application may come from a correlation evidenced between the diameter of nanoparticles catalyzing the growth of carbon nanotubes (CNTs) and the final diameter of CNTs synthesized via chemical vapor deposition (CVD) [6–8]. From this correlation, many studies have been completed to produce narrower distributions of catalytic particle radii in the hope of narrowing the diameter distribution of any CNTs synthesized later. Much of this research has been focused on reducing the mean size of the particles and, consequently, by applying simple statistics, a narrower size distribution [9]. Regardless of application, some measure of control over nanoparticle size and spacing is desired, however, the methods presented thus far are often time, equipment, and labor-intensive processes for producing ideal or near-ideal distributions for particle size and spatial order.

One strategy to create and organize structures at the nanoscale is to harness the inherent self-assembly mechanisms of a material. The physical properties of liquid metals, such as low viscosity and high surface energy, make it a prime material to produce self-assembled metallic nanostructures [10]. Dewetting is a process that uses the self-assembly mechanisms of a material to transform a homogeneous, metastable thin film into a series of nanoparticles through rapid thermal annealing, such as solid-state dewetting [11], which is also seen with solar cells [12], or pulsed laser-induced dewetting (PLiD) [13, 14]. We propose that

This manuscript has been authored by UT-Battelle, LLC under Contract No. DE-AC05-00OR22725 with the US Department of Energy. The United States Government retains and the publisher, by accepting the article for publication, acknowledges that the United States Government retains a non-exclusive, paid-up, irrevocable, world-wide license to publish or reproduce the published form of this manuscript, or allow others to do so, for United States Government purposes. The Department of Energy will provide public access to these results of federally sponsored research in accordance with the DOE Public Access Plan (http://energy.gov/downloads/doe-public-access-plan).

✉ Nicholas A. Roberts
nick.roberts@usu.edu

[1] Department of Mechanical and Aerospace Engineering, Utah State University, Logan, UT, USA

[2] Center for Nanophase Materials Science, ORNL, Oak Ridge, TN, USA

[3] Department of Materials Science, University of Tennessee, Knoxville, TN, USA

Published online: 10 February 2018

the dewetting phenomena in thin, metal films may hold an answer to reducing the diameter and pitch distributions of nanoparticles in an in situ, self-assembled, scalable process.

Examples of dewetting for spatial control of nanoparticles already include probe-assisted dewetting, laser-assisted dewetting or PLiD [15], pre-patterning of substrates [16, 17], e-beam assisted dewetting, and a few more [18]. Other methods for spatial control that use more scalable manufacturing techniques have been evidenced using confinement or sacrificial films [19]. A recent article demonstrates a simple and robust method for spatial control with the ability to manufacture ordered metallic nanoparticle arrays via reduction of polymeric-metallic compounds [20]. Typical films are dewet with a free vertical surface and have their final morphology dictated by a Rayleigh–Plateau-like instability that is dependent on minimizing the surface free energy of the sample [11, 21, 22]. These instabilities are greatly affected by the relative surface energies of the materials involved, indicating that adjustments to these surface energies could alter final morphology of nanoparticles fabricated via dewetting.

A simple method to alter surface energies of dewetting films would be the addition of a capping layer on top of the metastable thin metal film. For example, confinement techniques have been seen to produce highly ordered arrays of nanoparticles in certain regions of a polymer film, but not for an entire sample [23]. Farzinpour et al. studied the impact of the addition of a sacrificial antimony layer under a dewetting gold film of varying thickness and observed a tunable increase in particle size [19]. This method exhibited good manufacturing techniques and a large amount of control, but was limited to only increasing the size of the particles with the addition of these sacrificial layers. Sundar et al. also used a contact foil during a dewetting process to remove some gold from the nanoparticles produced [24]. This has the effect of reducing the nanoparticle size, but is not an additive process, consequently, the spacing between particles was increased as the gold was removed. Another investigation shows a suppression of dewetting using a capping layer [25], indicating that capping layers could be used to alter the instabilities affecting the film during the dewetting process.

The previous studies have shown that alterations in film surface energies can significantly alter the final distributions of nanoparticles formed via dewetting. In the present work, we investigate a method for size and spatial control of metallic nanoparticles by altering the surface energy of dewetting thin Ni films through the addition of a variable thickness alumina (Al_2O_3) capping layer. The alterations to the surface energy change the kinetics of the dewetting process and produce particle arrays of altered size and spacing. The major benefits to this method, as opposed to others, is that it offers a method for nanoparticle control without the time, equipment, and labor-intensive processing steps required by existing techniques. Thus, it is a step toward a scalable technique for control of nanoparticle size and spatial distributions.

2 Experimental methods

2.1 Ni samples

Samples were fabricated in a class 1000 cleanroom environment at the Center for Nanophase Materials Science at Oak Ridge National Laboratories (ORNL) using RCA clean Si wafers with a 100-nm thick thermally grown oxide. Samples had a 5-nm thick Ni film deposited via DC magnetron sputtering using an AJA International-ATC 2400 Sputtering System. The samples then had one of four different thickness, (0, 5, 10, 20) nm, Al_2O_3 films deposited by atomic layer deposition (ALD) using an Oxford Instruments FlexAl ALD system.

The dewetting process for the Ni-Al_2O_3 system was carried out using a pulsed, KrF excimer laser, with a wavelength of 248 nm, pulse-width of 18 ± 2 ns at full-width-at-half-max, with only one pulse delivered per sample. The area of the laser spot is ~ 1 cm^2 with a fluence of 250 ± 10 mJ/cm^2, which is sufficient to melt the Ni film [26].

The samples were then etched in a 3:1:1= H_2O:NH_4OH:H_2O_2 solution at 80 °C to remove the remaining Al_2O_3. Each of the experimental samples were etched twice and imaged via Scanning Electron Microscope (SEM) before and after each etch. Each of the etch processes for the Ni-Al_2O_3 system was carried out for 3 h. Energy dispersive X-ray spectroscopy (EDX) was also used to confirm that Al_2O_3 can be removed and that the larger particles (shown in images in the results section) were composed of Al_2O_3, and not Ni.

CNT growth was performed in a quartz tube, with feedstock flow of H_2:Ar:C_2H_4 = 100:80:20 sccm at 750 °C for 15 min. CNT growth is typically done using thinner catalytic films than the 5-nm thick Ni films used here. The choice of thickness was predicated upon producing a continuous film via sputtering that, once dewet, would have particles of a size that would be easy to image as well as be large enough to show evidence of changes to particle array statistics. To investigate some of the properties of as-grown CNTs, Raman spectroscopy was performed using a Renishaw in-via Raman Microscope with a 633-nm HeNe laser.

2.2 Morphology investigation

The surface morphology of the films and any as-grown CNTs was investigated with the use of a FEI Quanta FEG SEM. The particle sizes extracted from any SEM images were analyzed using a Monte Carlo Search Method in a

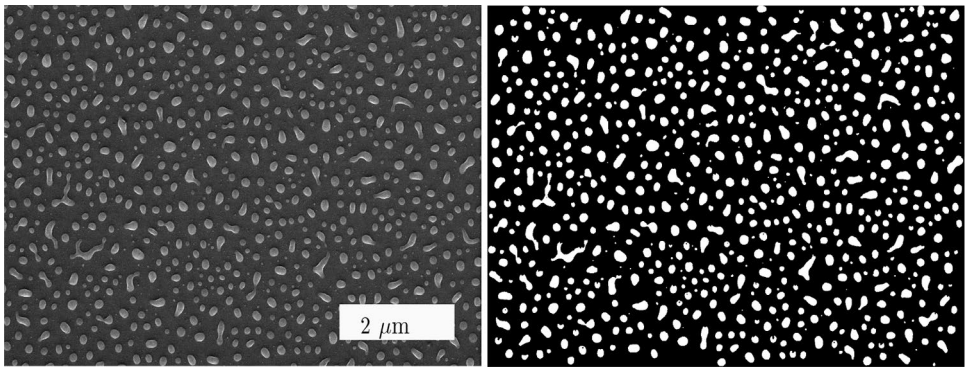

Fig. 1 The left panel illustrates an SEM image taken of Ni NPs. The right panel illustrates the image after the thresholding, edge removal, particle filling and noise reduction processes from the nanoparticle analyzer

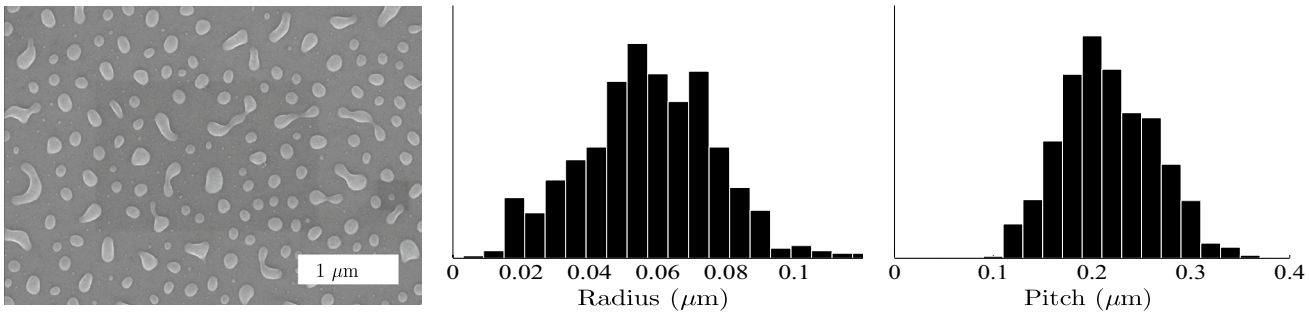

Fig. 2 The SEM image and the distributions for radii and pitch for the control

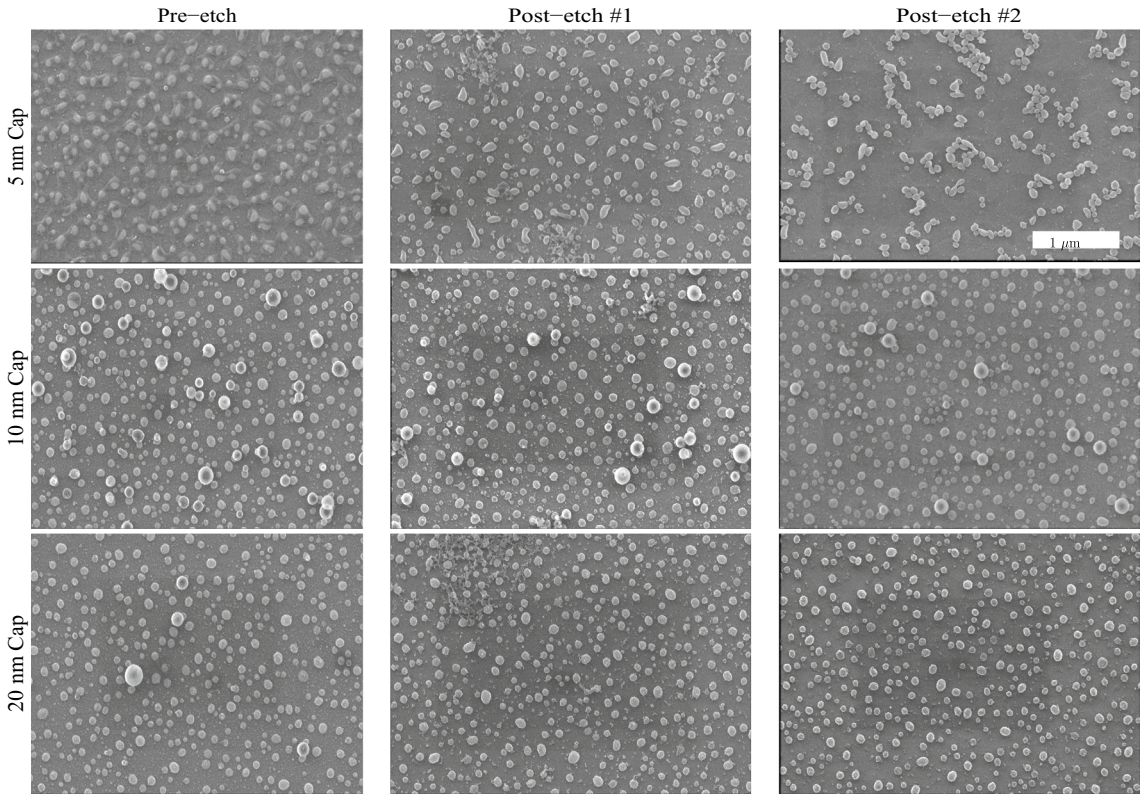

Fig. 3 The SEM images for all three capping layer thicknesses before and after the etches

nanoparticle analyzer [15]. The nanoparticle analyzer produces a list of radius and pitch for all particles in the SEM image. The pitch is calculated based on the distance from every particle and the particle nearest to it, therefore, being an indicator of particle spacing. An example of the modifications the analyzer makes to the SEM images is presented in Fig. 1 for the case of no capping layer.

In this figure several processes have been completed going from the standard SEM image to the black and white image. The image has already been cropped to remove the scale bar. Any particles on the edge of the image that are not complete have already been removed. The image was then set to a threshold to convert the greyscale image to black and white. Noise reduction and particle filling routines were run multiple times to achieve the best match with the initial SEM image. For the cases where there is an Al_2O_3 capping layer, the cropping function was used to manually reduce the areas that are being analyzed to not include the large Al_2O_3 particles and then iterated through the image to include all possible Ni nanoparticles.

3 Results and discussion

The control sample for this study was the case of no capping layer. An SEM image along with representative radii and pitch distributions for the control sample can be seen in Fig. 2. For the cases with a capping layer, SEM images and their corresponding radii and pitch distributions, before and after each of the two etches, can be found in Figs. 3, 4 and 5, respectively. For reference, all SEM images presented in this section were taken at a magnification of 50 kX, with a scale bar of 1 μm.

For the case where the capping layer is 5 nm thick, the initial etch appears to have removed the majority of the Al_2O_3 with the second etch removing any small Al_2O_3 particles from the surface. The second etch also appears to have allowed for the migration of NPs at the elevated temperature of 80 °C during the etch, indicating that only one etch is necessary for this thickness. The final values presented for samples with a 5-nm cap were acquired from images taken prior to the second etch. This ensures that the particle

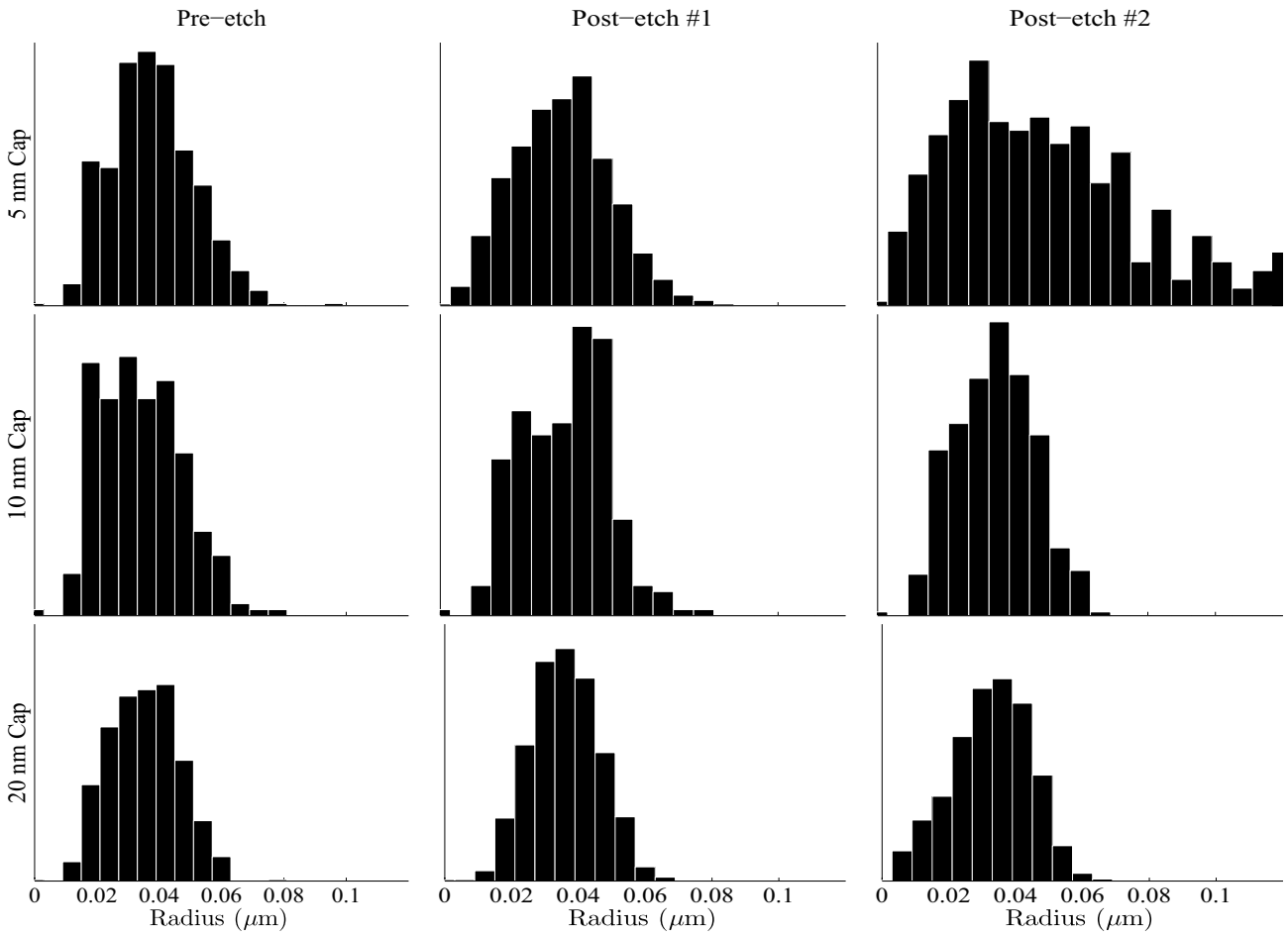

Fig. 4 The radii distributions for all three capping layer thicknesses before and after the etches

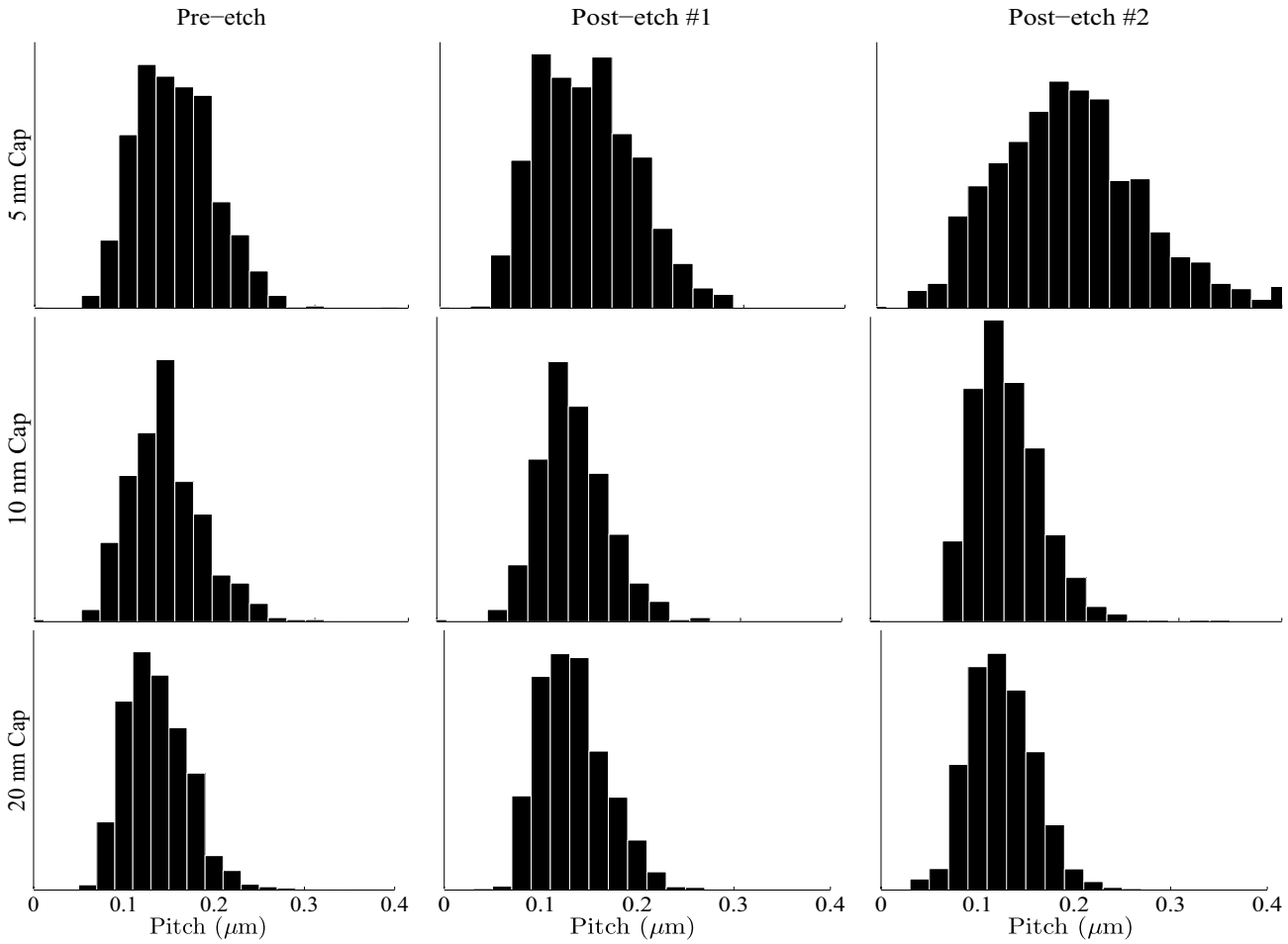

Fig. 5 The pitch distributions for all three capping layer thicknesses before and after the etches

agglomeration from the second etch does not influence the results for this case.

The set of particle radii and pitch obtained via the nanoparticle analyzer for each sample were then used to calculate a mean and standard deviation of all the Ni particles that were affected by the addition of capping layers. The radii and pitch distributions followed a Rayleigh-like distribution, which was expected as the dominant liquid-phase instability is similar to that of the Rayleigh–Plateau instability, which is also respresented by the Rayleigh distribution. Values illustrating trends in the mean and standard deviation with respect to capping layer thickness are presented in Table 1. From this table and figures of results, the reduction in particle size and distribution spread is evident. Final values from the table indicate that optimal results will be achieved for capping layer thicknesses of 10 and 20 nm. In each of these cases, the Al_2O_3 capping layers were also dewet, producing the larger particles shown in Fig. 3. EDX was used to confirm that these larger particles were Al-rich, while the remaining area was Al-depleted. However, upon examination of the SEM images for the case with the 10 nm cap, the etch does not appear to have removed all of the Al_2O_3 particles from the surface. The samples with the 20-nm capping layer are optimal for our investigation of CNT growth since they have less Al_2O_3 particles.

Table 1 Tabulated values for the means and standard deviations of the radii and pitch distribution for each of the four capping layer thicknesses

Cap thickness (nm)	$\bar{r}$ (nm)	s_r (nm)	$\bar{p}$ (nm)	s_p (nm)
0	57.1	19.5	216	47.6
5	36.0	14.0	145	47.8
10	34.8	11.6	134	34.5
20	32.6	11.7	124	34.2

SEM images after CNT growth can be seen in the top panel of Fig. 6. From these images, it is clear that the addition of a capping layer to reduce the nanoparticle size and

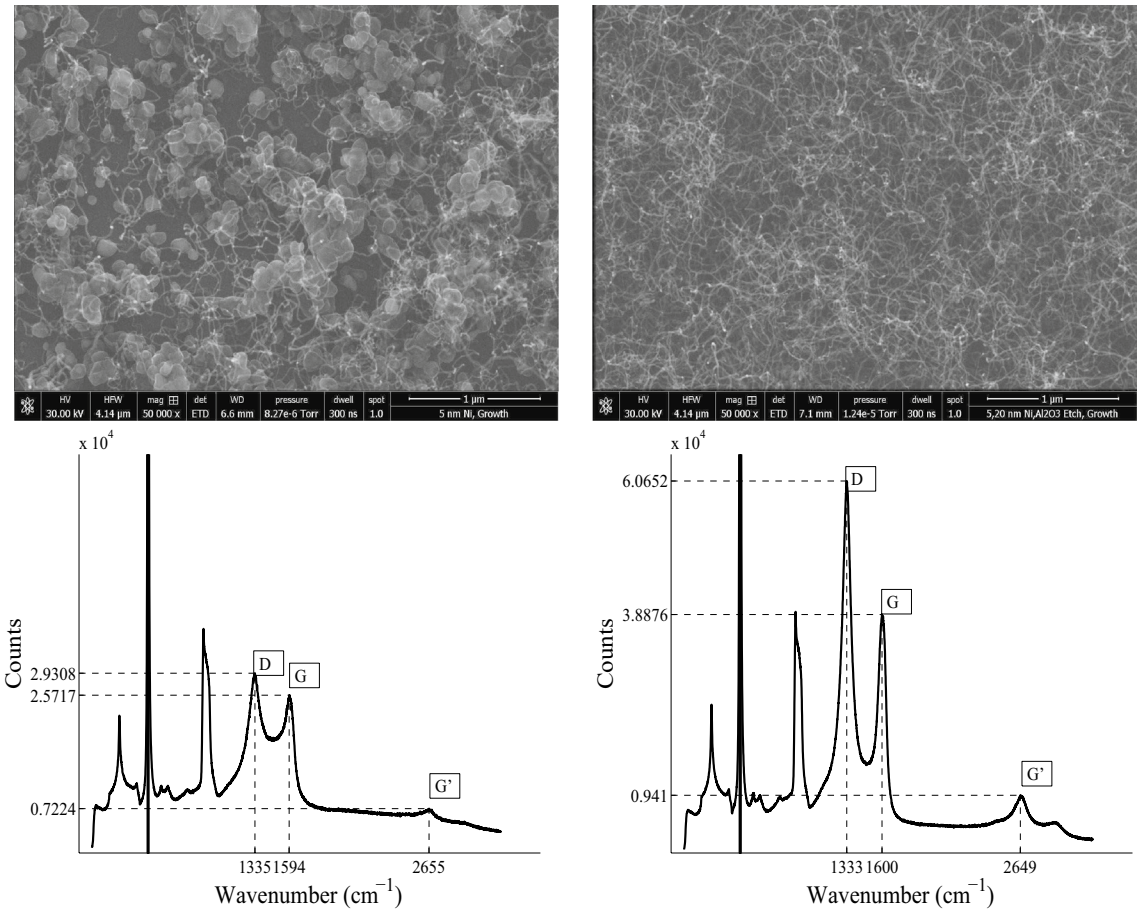

Fig. 6 SEM images and respective Raman spectra for an uncapped sample in the left panel and a 20-nm thick capped sample in the right panel after CNT growth

spacing has engendered a much different CNT mat than the control sample. The area density of the CNTs has increased greatly, with no evidence of nanoparticle agglomeration during the growth process. The increased CNT density is also reflected by the larger peaks that correspond to the CNTs, namely the labeled D, G, and G′ peaks in Fig. 6. Additional differences after growth can also be observed from the Raman spectra for each sample presented in the bottom panel of Fig 6. The first observation from the Raman spectra differences is the shift in the mode frequencies of the D band (1335 to 1333 cm^{-1}), G band (1594 to 1600 cm^{-1}), and the G′ band (2655 to 2649 cm^{-1}), that are a result of a decrease in the CNT diameter [27]. This is also indicated by the peak ratio of the D/G bands (11,369 for the uncapped sample and 15,601 for the capped sample), which shows a strong diameter dependence and increases with decreasing CNT diameters [28, 29].

4 Conclusion

Here, we have presented a new scalable process to alter the radii and pitch distributions of Ni nanoparticles, specifically one that offers a simple method to reduce particle sizes, and shown the differences in as-grown CNT mats. The mean and standard deviation of the size and spacing of the Ni nanoparticles were reduced with the addition of different thickness Al_2O_3 capping layers prior to dewetting. Analysis of the final nanoparticles shows approximately a 43% decrease in both the mean particle radii and pitch between particles for the optimum case. The standard deviation of particle radii was reduced by approximately 40% and the pitch standard deviation by approximately 28%.

The alterations in the particle distributions presented here are only a first step towards size and spacing control of self-assembled nanoparticles. However, this novel method presents a route to adjust the nanoparticle size and spacing distributions without the use of expensive or time-intensive process steps or a reduction in the metastable thin film thickness. This indicates

that we can now use self-organization techniques to produce NP array distributions that were not previously realizable.

Acknowledgements The material fabrication portion of this research was conducted at the Center for Nanophase Materials Sciences, which is a DOE Office of Science User Facility. We also acknowledge the support from the Microscopy Core Facility at Utah State University for the SEM results, which was acquired through support of the National Science Foundation (CMMI 1337932). PDR acknowledges support from the National Science Foundation (CBET 1603780—Ronald Joslin program manager) for his contribution to this work.

References

1. M. Segev-Bar, H. Haick, Flexible sensors based on nanoparticles. ACS Nano **7**, 8366–8378 (2013)
2. I. Wong, G. Teo, C. Neto, S. Thickett, Micropatterned surfaces for atmospheric water condensation via controlled radical polymerization and thin film dewetting. ACS Appl. Mater. Interfaces **7**, 21562–21570 (2015)
3. K. Nakayama, K. Tanabe, H.A. Atwater, Plasmonic nanoparticle enhanced light absorption in gaas solar cells. Appl. Phys. Lett. **93**, 121904 (2008)
4. H.A. Atwater, A. Polman, Plasmonics for improved photovoltaic devices. Nat. Mater. **9**, 205–213 (2010)
5. E. Destouesse, S. Chambon, S. Courtel, L. Hirsch, G. Wantz, Solution processed small-molecule bulk heterojunctions: leakage currents and the dewetting issue for inverted solar cells. ACS Appl. Mater. Interfaces **7**, 24663–24669 (2015)
6. Y. Li, W. Kim, Y. Zhang, M. Rolandi, D. Wang, H. Dai, Growth of single-walled carbon nanotubes from discrete catalytic nanoparticles of various sizes. J. Phys. Chem. B **105**, 11424–11431 (2001)
7. C. Cheung, A. Kurtz, H. Park, C. Lieber, Diameter-controlled synthesis of carbon nanotubes. J. Phys. Chem. B **106**, 2429–2433 (2002)
8. A. Moisala, A. Nasibulin, E. Kauppinen, The role of metal nanoparticles in the catalytic production of single-walled carbon nanotubes—a review. J. Phys. Condens. Matter **15**, S3011–S3035 (2003)
9. A. Geissler, M. He, J.-M. Benolt, P. Petit, Effect of hydrogen pressure on the size of nickel nanoparticles formed during dewetting and reduction of thin nickel films. J. Phys. Chem. C **114**, 89–92 (2010)
10. P. Rack, Y. Guan, J. Fowlkes, A. Melechko, M. Simpson, Pulsed laser dewetting of patterned thin metal films: a means of directed assembly. Appl. Phys. Lett. **92**, 223108 (2008)
11. C.V. Thompson, Solid-state dewetting of thin films. Annu. Rev. Mater. Res. **42**, 399–434 (2012)
12. F. Beck, S. Mokkapati, K. Catchpole, Plasmonic light-trapping for Si solar cells using self-assembled, Ag nanoparticles. Prog. Photovolt. Res. Appl. **18**, 500–504 (2010)
13. J. Fowlkes, Y. Wu, P. Rack, Directed assembly of bimetallic nanoparticles by pulsed-laser-induced dewetting: a unique time and length scale regime. ACS Appl. Mater. Interfaces **2**, 2153–2161 (2010)
14. J. Fowlkes, L. Kondic, J. Diez, Y. Wu, P. Rack, Self-assembly versus directed assembly of nanoparticles via pulsed laser induced dewetting of patterned metal films. Nano Lett. **11**, 2478–2485 (2011)
15. N. Roberts, J. Fowlkes, K. Mahady, S. Afkhami, L. Kondic, P. Rack, Directed assembly of one- and two-dimensional nanoparticle arrays from pulsed laser induced dewetting of square waveforms. ACS Appl. Mater. Interfaces **5**, 4450–4456 (2013)
16. Y. Wu, J.D. Fowlkes, P.D. Rack, J.A. Diez, L. Kondic, On the breakup of patterned nanoscale copper rings into droplets via pulsed-laser-induced dewetting: competing liquid-phase instability and transport mechanisms. Langmuir **26**, 11972–11979 (2010)
17. Y. Wu, N. Dong, S. Fu, J. Fowlkes, L. Kondic, M. Vincent, D. deCeglia, Directed liquid phase assembly of highly ordered metallic nanoparticle arrays. ACS Appl. Mater. Interfaces **6**, 5835–5843 (2014)
18. D. Gentili, G. Foschi, F. Valle, M. Cavallini, Application of dewetting in micro and nanotechnology. Chem. Soc. Rev. **41**, 4430–4443 (2012)
19. P. Farzinpour, A. Sundar, K. Gilroy, Z. Eskin, R. Hughes, S. Neterina, Alterign the dewetting characteristics of ultrathin gold and silver films using a sacrificial antimony layer. Nanotechnology **23**, 495604–495614 (2012)
20. X. Han, J. Hou, J. Xie, J. Yin, Y. Tong, C. Lu, H. Mohwald, Synergism of dewetting and self-wrinkling to create two-dimensional ordered arrays fo functional microspheres. ACS Appl. Mater. Interfaces **8**, 16404–16411 (2016)
21. R. Baluffi, S. Allen, W. Carter, *Kinetics of materials* (Wiley, Hoboken, 2005)
22. Y. Wu, Nanoscale metal thin film dewetting via nanosecond laser melting: understanding instabilities and materials transport in patterned thin films. PhD Thesis, University of Tennessee, Knoxville (2011)
23. J. Peng, R. Xing, Y. Wu, B. Li, Y. Han, W. Knoll, D. Kim, Dewetting of thin polystyrene films under confinement. Langmuir **23**, 2326–2329 (2007)
24. A. Sundar, R. Hughes, P. Farzinpour, K. Gilroy, G. Devenyi, J. Preston, S. Neretina, Manipulation the size distribution of supported gold nanostructures. Appl. Phys. Lett. **100**, 013111 (2012)
25. J.E. Kline, Suppression of dewetting in pulsed laser melting of thin metallic films on silica. PhD Thesis, Washington University (2005)
26. Y. Guan, R. Pearce, A. Melechko, D. Hensley, M. Simpson, P. Rack, Pulsed laser dewetting of nickel catalyst for carbon nanofiber growth. Nanotechnology **19**, 235604–235607 (2008)
27. H. Nii, Y. Sumiyama, H. Hakagawa, A. Kunishige, Influence of diameter on the Raman spectra of multi-walled carbon nanotubes. Appl. Phys. Express **1**, 064005 (2008)
28. M.S. Dresselhaus, A. Jorio, A.G.S. Filho, R. Saito, Defect characterization in graphene and carbon nanotubes using Raman spectroscopy. Philos. Trans. R. Soc. A **368**, 5355–5377 (2010)
29. J. Hodkiewicz, *Rapid quality screening of carbon nanotubes with Raman spectroscopy* (Thermo Fisher Scientific, Application Note: 51947, 2010)